# Description of order-disorder transitions based on the phase-field-crystal model

Yunhao Huang, Jincheng Wang,* Zhijun Wang, Junjie Li, and Can Guo
*State Key Laboratory of Solidification Processing, Northwestern Polytechnical University, Xi'an 710072, People's Republic of China*
(Received 16 August 2016; revised manuscript received 2 January 2017; published 25 April 2017)

Order-disorder transition is an attractive topic in the research field of phase transformation. However, how to describe order-disorder transitions on atomic length scales and diffusional time scales is still challenging. Inspired from high-resolution transmission electron microscopy, we proposed an approach to describe ordered structures by introducing an order parameter into the original phase-field-crystal model to reflect the atomic potential distribution. This new order parameter contains information about kinds of atoms, showing that different kinds of sublattices in ordered structures can be distinguished by the amplitude of the order parameter. Two case studies, growth of ordered precipitations and evolution of antiphase domains, are also presented to demonstrate the capabilities of this approach.

DOI: 10.1103/PhysRevE.95.043307

## I. INTRODUCTION

Ordered structures, crystalline solids with regular periodic lattices, widely exist in microstructures of materials, for example, $L1_2$ phase in the nickel-based superalloys and $B2$ phase in the Cu-Zn alloys [1]. These alloys are in a disordered state at high temperatures but form ordered superlattices at low temperatures. Order-disorder transitions are always an attractive topic in the research field of phase transformation. Plenty of research has focused on the kinetics of ordering processes [2,3], strengthening mechanisms, deformation behaviors of ordered phases [4,5], etc.

In past decades, many theoretical models have been proposed to describe order-disorder phase transitions, such as the Bragg-Williams-Gorsky approximation [6,7], and the cluster variation method [8]. However, these phenomenological theories of ordering take into account only interactions of the nearest- and/or the next-nearest-neighbor atoms rather than long-range interactions which is essential in order-disorder transitions. On the other hand, order-disorder phase transitions involve structure changes that couple atomic-scale knowledge of structures with chemical composition diffusional processes, which makes it very difficult to describe phase transformations by these phenomenological theoretical models [9].

With the development of computational materials science, many computer simulation methods are also employed to deal with order-disorder phase transitions, such as the continuum phase-field model [10,11] and the molecular-dynamics method [8]. However, although phase-field studies can formulate the free-energy function of ordered structures, this method washed out most of the relevant atomic-scale physics [10,11]. So the phase-field model cannot deal with the kinetics of ordering processes on atomic scales, as well as strengthening mechanisms and deformation behaviors of ordered phases. As to the molecular-dynamics simulation, because of the very limited time step, presently it is impossible to simulate order-disorder phase transitions which occur on diffusional time scales. Therefore, there still remain some difficulties in describing order-disorder phase transitions on atomic length scales and diffusional time scales by using the existing simulation tools.

The phase-field-crystal (PFC) methodology, a variant of classical density functional theories, has recently emerged as an efficient and mathematically accessible option in the study of phase transitions on atomic length scales and diffusional time scales, incorporating with thermodynamics of phase transformation and most salient solid-state properties [12–19]. The PFC models have been applied to simulate complex structural transformations in binary and multicomponent alloys [14,20–22]. However, to date, the PFC models are not suitable for describing order-disorder transitions. For the original PFC model [13,23], it uses a single atom density field to describe arrangements of different atoms, which makes it incapable of distinguishing different kinds of atoms. The PFC model of vacancy for binary alloys [16,24–26], using two atom density fields to describe atom arrangements, can deal with arrangements of different kinds of atoms and ordered structures; however, this model only takes into account interactions of the nearest-neighbor atoms instead of the long-range interactions. Most recently, Alster and Elder [27] proposed a phase-field-crystal model for ordered phases by adding a periodic concentration field to the original binary PFC model. The work describes order-disorder transformations by adding the long-range information of ordered structures into the original order parameter in the PFC model. Besides, there is always another approach to describe the order-disorder system in the PFC model as we proposed in this work.

From the aspect of experiments, people can use high-resolution transmission electron microscopy (HRTEM) to determine whether a structure is ordered or not [28–31]. In HRTEM, different atomic potentials for different kinds of atoms result in different electron diffraction patterns and thus different intensities in HRTEM images [32]. So in practice, image intensities and diffraction patterns are used to distinguish ordered and disordered structures. A disordered phase has a random arrangement of atoms, so its diffraction pattern can only reflect the basis crystal lattice, resulting in a uniform HRTEM image intensity for different atoms. For an ordered structure, however, it has a periodic arrangement of atoms, so its diffraction pattern can show superlattice structures due to the difference in image intensity for different kinds of atoms.

In this work, inspired from HRTEM and taking the long-range interaction into account, we developed an approach to describe order-disorder phase transitions based on the PFC model. Through using an order parameter to reflect the atomic

*Corresponding author: jchwang@nwpu.edu.cn

 

potential distribution, different kinds of sublattices in ordered structures can be distinguished by the amplitude of the order parameter. Two case studies, growth of ordered precipitations and evolution of antiphase domains, are also conducted to demonstrate the capabilities of this approach.

## II. THE PFC MODEL FOR ORDER-DISORDER SYSTEM

### A. The original PFC model

The free-energy functional for the PFC model can be obtained from the classical density functional theory. In the classical density functional theory, the free energy of a binary system can be written as

$$\frac{\Delta F}{k_B T} = \frac{\Delta F_{\mathrm{id}}}{k_B T} + \frac{\Delta F_{\mathrm{ex}}}{k_B T}, \tag{1}$$

where $\Delta F_{\mathrm{id}}$ is an ideal energy responsible for driving the density to a uniform field, $\Delta F_{\mathrm{ex}}$ is an excess free-energy density which drives the density field to form periodic structures, $k_B$ is the Boltzmann constant, and $T$ stands for temperature. $\Delta F_{\mathrm{id}}$ is the sum of the ideal free energy of individual fields $\rho_A$ and $\rho_B$:

$$\frac{\Delta F_{\mathrm{id}}}{k_B T} = \rho_A \ln\frac{\rho_A}{\rho_A^0} - \delta\rho_A + \rho_B \ln\frac{\rho_B}{\rho_B^0} - \delta\rho_B. \tag{2}$$

Here $\rho_A$ and $\rho_B$ are the individual local atomic density fields of components $A$ and $B$, respectively. The total atomic density is defined as $\rho = \rho_A + \rho_B$ and the sum of the two reference densities of the system is defined as $\rho^0 = \rho_A^0 + \rho_B^0$, where $\rho_A^0$ and $\rho_B^0$ are two independent reference states of $A$ and $B$, respectively. We also defined a solute concentration as $c = \rho_B/(\rho_A + \rho_B)$ and a reference composition as $c_0 = \rho_B^0/(\rho_A^0 + \rho_B^0)$. The total mass density $\rho$ can be further simplified as a dimensionless density field $n = \rho/\rho^0 - 1$. Then the ideal free-energy density of Eq. (2) can be recast as

$$\frac{\Delta F_{\mathrm{id}}}{k_B T \rho^0} = (n+1)\ln(n+1) - n + (n+1) \times \left[ c \ln\frac{c}{c_0} + (1-c)\ln\frac{1-c}{1-c_0} \right]. \tag{3}$$

The excess free-energy density $\Delta F_{\mathrm{ex}}$ can be expanded by using a two-point correlation function to describe $A$-$A$, $B$-$B$, and $A$-$B$ interactions,

$$\Delta F_{\mathrm{ex}} = \sum_{i=A,B;\, j=A,B} \Delta F_{ij} = -\frac{1}{2} \sum_{i=A,B;\, j=A,B} \delta\rho_i(r) \times \int dr' C_2^{ij}(|r-r'|)\delta\rho_i(r'), \tag{4}$$

where $C_2^{ij}$ describes the correlation of components $i$ and $j$. As discussed in the work by Greenwood *et al.* [23], the solute concentration $c$ is a variable which has a much larger length scale compared with the periodicity of density field $n$. So we can make an approximation of $c(r') = c(r)$. Then Eq. (1) can be rewritten as

$$\frac{\Delta F[n(\vec{r})]}{kT\rho^0} = \int dr \frac{n(\vec{r})^2}{2} - \lambda\frac{n(\vec{r})^3}{6} + \chi\frac{n(\vec{r})^4}{12} + (n+1)\omega\left\{ c\ln\frac{c}{c_0} + (1-c)\ln\frac{1-c}{1-c_0} \right\} - \frac{1}{2}n\left[ \int dr' C_{\mathrm{eff}}^{n}(|r-r'|)n' + \int dr' C_{\mathrm{eff}}^{c}(|r-r'|)c' \right] - \frac{1}{2}(c-c_0)\left[ \int dr' C_{\mathrm{eff}}^{c_0 n}(|r-r'|)n' + \int dr' C_{\mathrm{eff}}^{c_0 c}(|r-r'|)c' \right]. \tag{5}$$

Here, $\lambda$ and $\chi$ are coefficients to fit the ideal energy to a polynomial expansion. The correlation functions in $\Delta F_{\mathrm{ex}}$ are modulated by the composition as

$$\begin{aligned} C_{\mathrm{eff}}^{n} &= c^2 C_2^{BB} + (1-c)^2 C_2^{AA} + c(1-c)\left(C_2^{BA} + C_2^{AB}\right), \\ C_{\mathrm{eff}}^{c} &= c\left(C_2^{BB} - C_2^{BA}\right) - (1-c)\left(C_2^{AA} - C_2^{AB}\right), \\ C_{\mathrm{eff}}^{c_0 n} &= c\left(C_2^{BB} - C_2^{AB}\right) - (1-c)\left(C_2^{AA} - C_2^{BA}\right), \\ C_{\mathrm{eff}}^{c_0 c} &= C_2^{BB} + C_2^{AA} - \left(C_2^{BA} + C_2^{AB}\right). \end{aligned} \tag{6}$$

From the derivation of the binary PFC model, we find that, the order parameter $n$ only can reflect the sum of occupation probability but without any information of atomic kinds; meanwhile, the concentration field $c$, as a long-range variable, does not contain information about the arrangement of atoms, either. So the original PFC model cannot describe ordered structures directly. To describe the order-disorder system, the kinds of atoms must be taken into account.

### B. The order parameter reflecting atomic potentials

On the one hand, the light spots in HRTEM images can be used to determine atomic positions and fundamental lattices. On the other hand, the image intensities in HRTEM images can be used to distinguish ordered and disordered structures because the image intensities are different between superlattices of ordered structures but uniform for disordered structures. These characteristics of HRTEM images inspire us that we can add a new order parameter into the PFC model to describe ordered structures, using the peak of the order parameter to reflect the fundamental lattice and the different peak heights to describe different superlattices. From the principle of HRTEM, we know that HRTEM images result from the atomic potential distributions [32]. This inspires us that atomic potential distribution is an applicable order parameter to describe the order-disorder system. The atomic potential distribution contains the information of the fundamental lattice and the difference between the superlattices as well as HRTEM images. So here we introduced a new order parameter $\eta$ into the PFC model to reflect the atomic potential distribution.

For the basis properties of crystal, there is an intrinsic relationship between the atomic potential distribution and atomic density, $\eta = G(n)$, where $G$ is a function related to kinds of atoms. Here, we do not aim to find out such a kernel $G$ from first principles, but rather apply the simplest possible

form of $\eta$ phenomenologically from the actual physical system. Ordered structures are periodic systems with two kinds of periodic lattices: one for the fundamental lattice (bcc, fcc, hcp, etc.) and the other for the regular arrangements of atoms. The atomic potential distribution $\eta$ of ordered structures contains the information of regular arrangements of atoms, which is the principle for HRTEM to discern the ordered structure. So $\eta$ of ordered structures can reflect the regular arrangements of atoms. For disordered structures, we treat disordered structures as a homogeneous state as the original PFC model did. This means that the atomic potential distribution $\eta$ of disordered structures only contains the period for the fundamental lattice. So $\eta$ includes the periods of the fundamental lattice in both ordered and disordered structures and the information about the regular arrangements of atoms in ordered structures. Thus $\eta$ can be used to describe order-disorder systems.

In the following, taking an $AB$ ordered alloy with a two-dimensional (2D) square lattice as examples, in which the structure can be divided into two sublattices $\alpha$ and $\beta$, as shown in Fig. 1(a), we show how the form of $\eta$ is constructed. In such a bipartite framework, all $A$ atoms reside on $\alpha$ sites, while all $B$ atoms reside on $\beta$ sites in the ordered ground state. The total $\eta$ of the ordered structure can be written as

$$\eta(r) = G[n(r)] = G_A[n_A(r)] + G_B[n_B(r)], \tag{7}$$

where $n(r) = n_A(r) + n_B(r)$. $n_A = (\rho_A - \rho_A^0)/\rho^0$ and $n_B = (\rho_B - \rho_B^0)/\rho^0$ are the densities of the $A$ and $B$ atoms, respectively, and

$$G = \begin{cases} G_A & \text{if atom} = A \\ G_B & \text{if atom} = B \end{cases} (G_A \neq G_B).$$

For a regular arrangement, $n_A$ and $n_B$ have the same form but a half cycle of phase shift between them in the 2D square lattice, as shown in Fig. 1(b). Values of $\eta$ on $\alpha$ sites and on $\beta$ sites are different due to the difference between $G_A$ and $G_B$. The difference of $\eta$ values on different sublattices is periodic, which reflects the regular arrangements of atoms. Therefore, the ordered structure can be described and different sublattices can be distinguished through the difference of $\eta$ in an ordered structure. As for a disordered structure, $A$ and $B$ atoms randomly reside on the lattices, which means that all lattice sites are randomly occupied by $A$ or $B$ atoms. So, in this case, $\eta$ only contain the period for the fundamental lattice as shown in Fig. 1(c).

### C. The free-energy functional

To construct the free-energy functional $F(\eta)$ of the system, in this work, we use the simplified free-energy functional derived by Greenwood *et al.* [23]:

$$\frac{\Delta F[\eta(\vec{r})]}{kT\rho^0} = \int \left\{ \frac{\eta(\vec{r})^2}{2} - \lambda\frac{\eta(\vec{r})^3}{6} + \chi\frac{\eta(\vec{r})^4}{12} + (\eta+1)\Delta F_{\text{mix}} - \frac{1}{2}\eta\int dr' C_{\text{eff}}^n(|r-r'|)\eta' + \frac{\varsigma}{2}|\vec{\nabla}c|^2 \right\} dr, \tag{8}$$

$$\Delta F_{\text{mix}} = \omega\left\{ c\ln\left(\frac{c}{c_0}\right) + (1-c)\ln\left(\frac{1-c}{1-c_0}\right)\right\}, \tag{9}$$

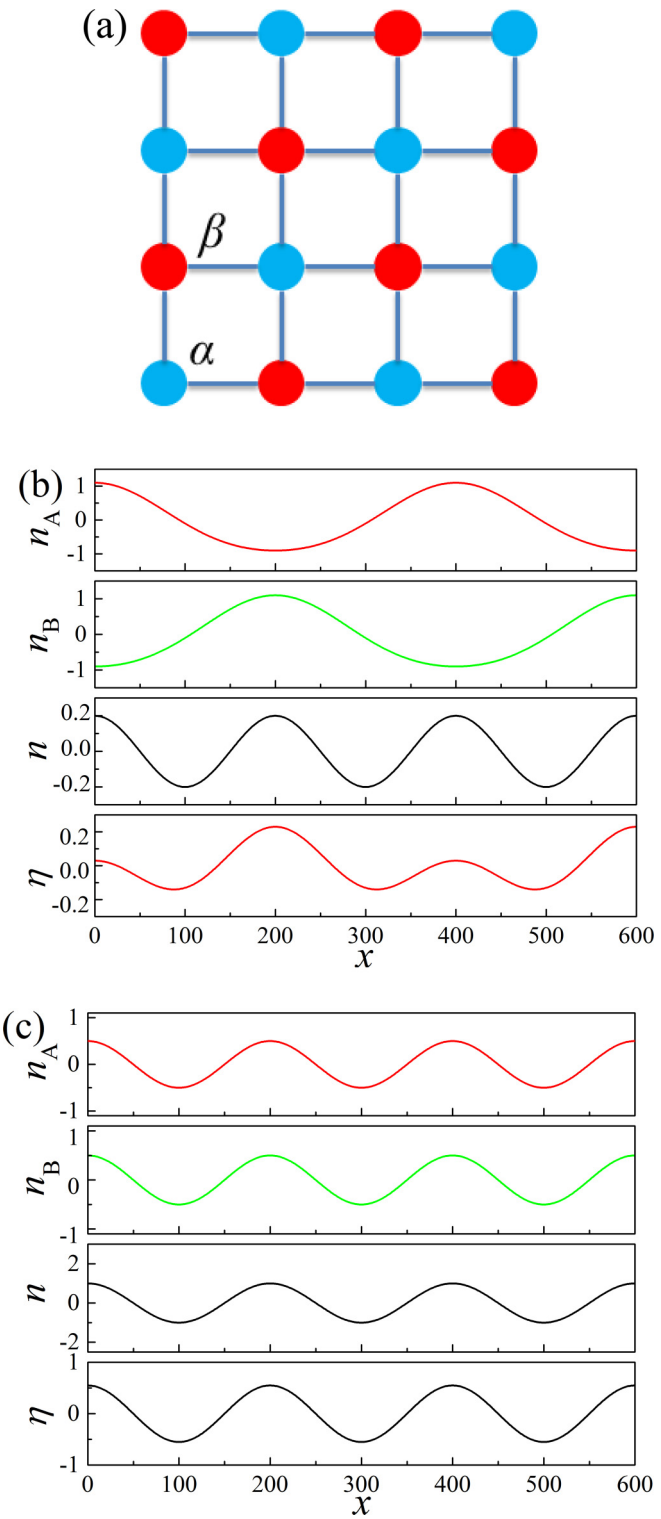


FIG. 1. (a) The ordered ground state of an $AB$ alloy on a square lattice, where blue and red circles represent the two kinds of atoms. Density fields $n_A(r)$, $n_B(r)$, $n(r)$ and the atomic potential distribution fields $\eta(r)$ in an ordered structure (b) and a disordered structure(c).

where $\Delta F_{\text{mix}}$ stands for the free energy of mixing. The coefficient $\omega$ is introduced to fit the entropic energy of mixing from the reference composition $c_0$, while the parameter $\varsigma$ is a coefficient that sets the energy of compositional interfaces.

Before introducing the correlation function $C^n_{\rm eff}(|r-r'|)$, first we will show how $\eta$ behaves in the order-disorder transition. The function form of $\eta$ can be written in terms of the reciprocal lattice vector mode,

$$\eta = \sum_j A_j e^{i\vec{k_j}\cdot\vec{r}} + \sum_m B_m e^{i\vec{k_m}\cdot\vec{r}} + \text{c.c.}, \qquad (10)$$

where c.c. is the complex conjugate, $\vec{k_j}$ and $\vec{k_m}$ are the fundamental reciprocal lattice vectors of the basis crystal and of the superlattice, respectively, and $A_j$ and $B_m$ represent the amplitudes of a given reciprocal lattice vector mode. In three dimensions, $\vec{k_j}$ and $\vec{k_m}$ can be written as $\vec{k} = n_1\vec{q_1} + n_2\vec{q_2} + n_3\vec{q_3}$, where ($\vec{q_1}$, $\vec{q_2}$, $\vec{q_3}$) are the principle reciprocal lattice vectors and $n_1$, $n_2$, $n_3$ are integers. For example, for a $B2$ ordered structure, the integers for the fundamental reciprocal lattice vector $\vec{k_j}$ are (1,1,0), and that for the ordered vector $\vec{k_m}$ is (1,1,1). (In this study, we only considered the most dominant peak.) However, for a disordered bcc structure, it only contains the fundamental reciprocal lattice vector $\vec{k_j}$. That is to say, $B_m = 0$ in disordered structures. During the precipitation of the ordered structure, $B_m$ changes from zero to nonzero.

As discussed above, the difference in the amplitude of $\eta$ between ordered and disordered structures is caused by the two-particle direct correlation function $C^n_{\rm eff}(|r-r'|)$. Therefore, considering the difference of $\eta$ between ordered and disordered structures, we introduced a correlation function as

$$C^n_{\rm eff}(|r-r'|) = X_{\rm basis}(c)C_2^{\rm basis} + X_{\rm order}(c)C_2^{\rm order}, \qquad (11)$$

where $C_2^{\rm basis}$ is the correlation function representing the contribution of the fundamental lattice to the excess free energy, and $C_2^{\rm order}$ is the contribution of the ordered part. $C_2^{\rm basis}$ acts on the fundamental lattice $\sum_j A_j e^{i\vec{k_j}\cdot\vec{r}}$ part and $C_2^{\rm order}$ works on the part of $\sum_m B_m e^{i\vec{k_m}\cdot\vec{r}}$. Because the ordered structure only exists when the concentration is close to $c_{\rm order}$ (the equilibrium concentration of ordered phase), a range limitation of $C_2^{\rm order}$ should be added into Eq. (11) as $X_{\rm order}(c)$. Here, we introduce the interpolation function $X_{\rm order}(c) = \xi e^{-(c-c_{\rm order})^2/\beta}$, where $\xi$ and $\beta$ are the height and width of the interpolation function, respectively. The interpolation function $X_{\rm basis}(c)$ is introduced to describe the free-energy change of the fundamental lattice due to the change of concentration. In this study, $X_{\rm basis}(c) = 1 - 0.3c^2 + 0.2c^3$ is introduced to construct an isomorphous phase diagram.

In this model, we set $C_2^{\rm basis}$ and $C_2^{\rm order}$ in the Fourier space by a Gaussian peak [14],

$$\hat{C}_2(k)_i = e^{-\sigma^2/\delta} e^{-[(k-k_i)^2/2\alpha_i^2]}. \qquad (12)$$

Equation (12) contains two exponential terms. The first exponential term includes the effect of temperature where $\sigma$ plays the role of an effective temperature, and $\delta$ controls the difference of different reciprocal lattice vectors. The second exponential term sets the peak position of the reciprocal lattice vector $k_i$, which is corresponding to the reciprocal lattice vector in Eq. (10). $\sigma$ works as a temperature parameter via the modulation of the peak height of $\hat{C}_2(k)_i$. As $\sigma$ changes, the stable structure changes. Variation of the Gaussian peak width $\alpha$ can change the properties of interfaces, defects, and strain [14,33]. The effect of $\alpha$ on the interface properties will be discussed in Sec. III.

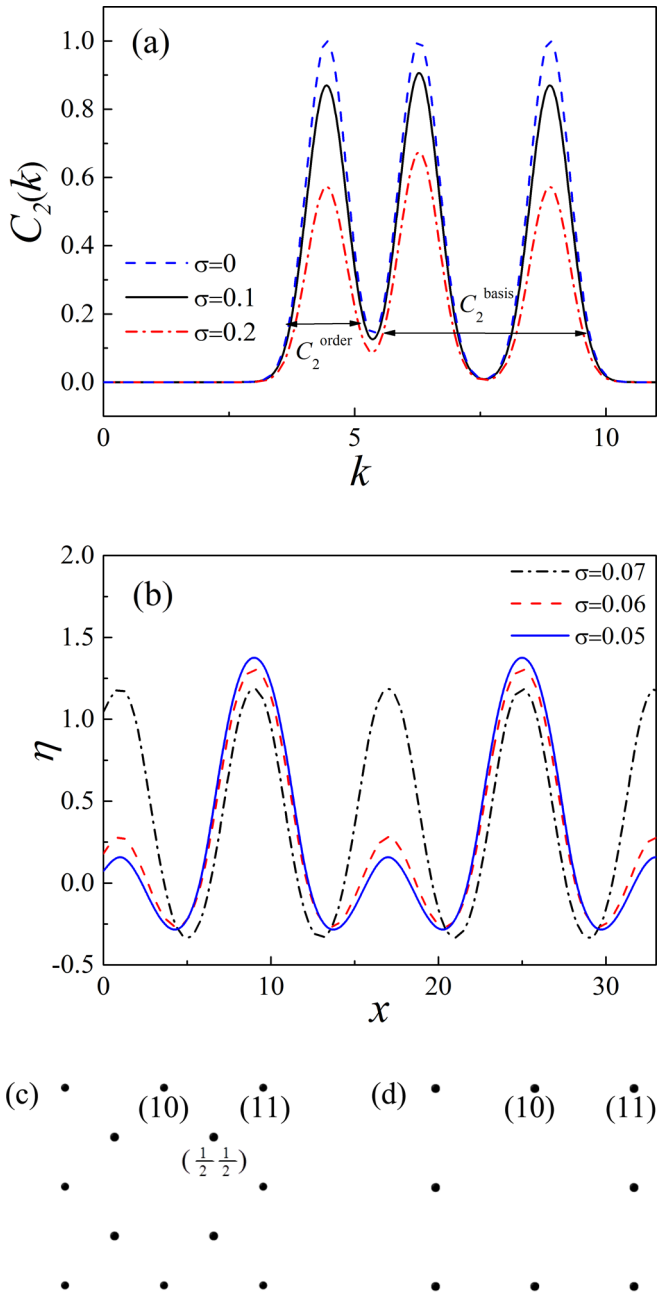


FIG. 2. (a) Direct pair correlation function for the order square phase with different temperature parameters $\sigma$ when $c = c_{\rm order} = 0.5$, where the first peak in the direct pair correlation shows the long-periodic arrangement and the latter two peaks show the basis crystal structure. (b) A comparison of $\eta$ between the ordered and disordered structures. When $\sigma = 0.7$, the stable structure is the disordered phase, while the ordered structure is stable for the other two cases. (c) and (d) show the spots of $\eta$ in Fourier space for the ordered and disordered structures, respectively. The spots of $\eta$ in (d) show the fundamental lattices [(1,0) and (1,1)], while those in (c) show a superlattice [$(\frac{1}{2},\frac{1}{2})$].

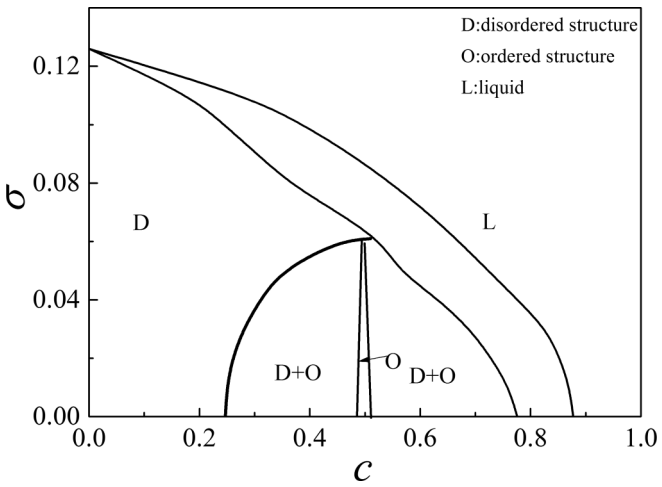


FIG. 3. Calculated phase diagram showing the coexistence between the ordered and disordered structures.

### D. Dynamics equations

Because $n_A$ and $n_B$ are conservative during phase transformation, $\eta$, the sum of $G_A(n_A)$ and $G_B(n_B)$, also should obey a conservative dynamics equation. The dynamics of order parameter field $\eta$ and concentration field $c$ obey the usual dissipative dynamics:

$$\frac{\partial \eta(\vec{r})}{\partial t} = M_\eta \nabla^2 \frac{\delta \Delta F}{\delta \eta(\vec{r})}, \tag{13}$$

$$\frac{\partial c(\vec{r})}{\partial t} = M_c \nabla^2 \frac{\delta \Delta F}{\delta c(\vec{r})}, \tag{14}$$

where $M_\eta$ and $M_c$ are kinetic mobilities of the order parameter $\eta$ and the concentration field $c$, respectively.

### E. Feasibility in order-disorder systems

In previous sections, we have discussed the free-energy functional, correlation functions, and dynamics equations. In this section, we will show the feasibility of our approach in order-disorder systems by the examples in 2D and 3D.

For a square lattice in 2D, it contains the fundamental reciprocal lattice vectors (1,0) and (0,1) and the superlattice reciprocal lattice vector $(\frac{1}{2},\frac{1}{2})$ corresponding to $k_1$, $k_2$, and $k_{\text{order}}$, respectively. In the present study, $k_1 = 2\pi/a_{\text{sq}}$, $k_2 = 2\pi\sqrt{2}/a_{\text{sq}}$, and $k_{\text{order}} = \sqrt{2}\pi/a_{\text{sq}}$, where $a_{\text{sq}} = 1$ (lattice constant of the fundamental lattice). To let the disordered state be stable at high temperatures but form ordered superlattices at low temperatures, we set $\delta_1 = 8$, $\delta_2 = 4\sqrt{2}$, and $\delta_{\text{order}} = 4$. Figure 2(a) shows the direct pair correlation function for a square ordered $AB$ alloy in 2D at $c = c_{\text{order}} = 0.5$ when $\sigma = 0$, 0.1, and 0.2. As shown in Fig. 2(a), there are three peaks of the direct pair correlation: the first peak, which has the lowest frequency, works on the superlattice reciprocal lattice vector $(\frac{1}{2},\frac{1}{2})$ and the latter two peaks work on the fundamental lattice vectors (1,0) and (0,1), respectively. In 2D, $\eta$ in Eq. (10) can be rewritten as

$$\eta = \eta_{10} + \eta_{11} + \eta_{\frac{1}{2}\frac{1}{2}}, \tag{15}$$

where $\eta_{10} = A_{10}[\cos(k_0 y) + \cos(k_0 x)]$, $\eta_{11} = A_{11}\cos(k_0 x)\cos(k_0 y)$, and $\eta_{\frac{1}{2}\frac{1}{2}} = A_{\frac{1}{2}\frac{1}{2}}\cos(k_0 x/2)\cos(k_0 y/2)$. As the temperature parameter $\sigma$ increases, the peak height of $\hat{C}_2(k)$ decreases and the ordered structure becomes stable. Then the amplitude difference of the two sublattices appears, as shown in Fig. 2(b). Figures 2(c) and 2(d) show the fast Fourier transform (FFT) images of the ordered and disordered structure, respectively. The spots in the FFT image of Fig. 2(d) show the fundamental lattices [(1,0) and (1,1)], while those of Fig. 2(c) show a superlattice $(\frac{1}{2},\frac{1}{2})$.

With the parameters mentioned above and through Eqs. (13)–(15), the phase diagram can be constructed from the free-energy curves for each bulk phase, as shown in Fig. 3. At high temperatures, liquid phase is the stable phase. As $\sigma$ decreases, the disordered phase separates out from the liquid. With the further decrease of temperature, the order-disorder transition occurs.

Similarly, the peak locations of the correlation functions for ordered structures in 3D also can be obtained by the diffraction theory: a reciprocal lattice has families of peaks derived from the interplanar spacings [14]. Table I shows the peak locations of the correlation functions [Eqs. (11) and (12)] in reciprocal space for several simple ordered structures: $B2$ and $L1_2$. Again, in 3D, Eq. (10) can be rewritten as

$$\eta = \eta_{111} + \eta_{200} + \eta_{100} + \eta_{110}, \tag{16}$$

where $\eta_{111} = A_{111}\sum_{h,k,l=\pm1}\cos[k_0(hx+ky+lz)]$, $\eta_{100} = A_{100}[\cos(k_0 x) + \cos(k_0 y) + \cos(k_0 z)]$, $\eta_{110} = A_{110}[\cos(k_0 x)\cos(k_0 y) + \cos(k_0 y)\cos(k_0 z) + \cos(k_0 x)\cos(k_0 z)]$, and $\eta_{200} = A_{200}[\cos(2k_0 x) + \cos(2k_0 y) + \cos(2k_0 z)]$. With Eq. (16) and the peak locations of correlation functions listed in Table I, ordered structures in 3D can be described. Figure 4 shows the simulated results of the $\eta$ field for the ordered structures of $B2$ and $L1_2$. The different colors of atoms in Fig. 4 reflect the different values of the $\eta$ field. The $B2$ structure can be seen as two overlapping simple cubic lattices. All $A$ atoms are on the simple cubic lattice $\alpha$ and all $B$ atoms are on the simple cubic lattice $\beta$. As shown in Fig. 4(a), on the slice of (110) face for $B2$, there are two corresponding rectangles for the two simple cubic lattices,

TABLE I. Lattice vectors and peaks locations of correlation functions in reciprocal space for ordered structures of $B2$ and $L1_2$.

| Order structures | Crystal structures | Fundamental lattice | | Superlattice | | |
|---|---|---|---|---|---|---|
| | | Index | $k$ | Index | $k_{\text{order}}$ | $c_{\text{order}}$ |
| B2 | BCC | (1,1,0) | $2\sqrt{2}\pi/a$ | (1,1,1) | $2\sqrt{3}\pi/a$ | 0.5 |
| $L1_2$ | FCC | (1,1,1) | $2\sqrt{3}\pi/a$ | (1,0,0) | $2\pi/a$ | 0.25 |
| | | (2,0,0) | $4\pi/a$ | | | |

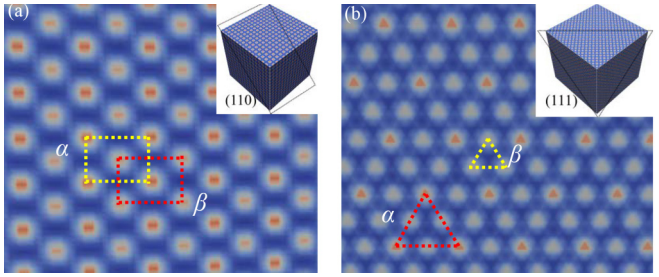


FIG. 4. Simulated results of the $\eta$ field for the ordered structures listed in Table I. (a) The slice of (110) face for $B2$ structures and (b) the slice of (111) for $L1_2$ structures. Different colors of atoms reflect different amplitudes of $\eta$ field. The rectangles in (a) and the triangles in (b) show the two kinds of superlattice in $B2$ and $L1_2$ structures, respectively.

respectively. The difference of $\eta$ between the two sublattices confirms the regular arrangements of atoms of the simulated results of $B2$. Similarly, the $L1_2$ structure can be seen as one simple cubic lattice $\alpha$ (all $A$ atoms on the vertex of fcc) and one octahedron lattice $\beta$ (all $B$ atoms on the face center of fcc). As shown in Fig. 4(b), on the slice of (111) face for $L1_2$, there are two corresponding triangles for the two sublattices. The differences of $\eta$ field between the two sublattices show the long-range periodicity of $L1_2$, too. The simulated results show that ordered structures in 3D also can be described by $\eta$ and the superlattices can be described by the amplitude difference between the two sublattices.

## III. APPLICATIONS

Here two case studies, growth of ordered precipitations and evolution of antiphase domains, are presented to demonstrate the capabilities of our approach in describing order-disorder phase transitions. Simulations were conducted in a domain of $1024 \times 1024$ with the dimensionless grid size $dx = 0.125$ and time step $dt = 0.001$. Dynamic equations, Eqs. (13) and (14), were solved semi-implicitly in the Fourier space with $M_\eta = 1$ and $M_c = 1$. The disordered matrix has an initial composition of $c = 0.47$ and that for the ordered domain is $c = 0.5$ at $\sigma = 0.02$.

### A. Precipitation

As we know, precipitation will happen when a supersaturated matrix is quenched into an order-disorder coexistence region in the phase diagram, which is one of the most important features for the order-disorder phase transition. So the first case study is about the growth of ordered precipitations. In the present study, a small spherical domain of ordered structure with a radius of $8a_{sq}$ was set in the center of the domain initially. Figures 5(a)–5(c) show the growth process of an ordered precipitation. It should be noted that, to get a better presentation, only one-quarter of the computational domain is shown in Figs. 5(a)–5(c). Through distinguishing the amplitude of $\eta$, we can differentiate between the ordered and disordered structures and the two sublattices in the ordered phase. From Figs. 5(a)–5(c), we also can see that the ordered phase grows through a layer-by-layer mode, i.e., first the atoms at plane (11) near the order-disorder phase boundary become ordered and form a step on the boundary near the ordered domain side; then the step moves forward resulting in the displacement of (11) layers. Figure 5(d) shows the variation of volume fraction for the precipitate with time. From this figure, we can find that the volume fraction of precipitate varies with time quadratically, indicating that the growth kinetics of

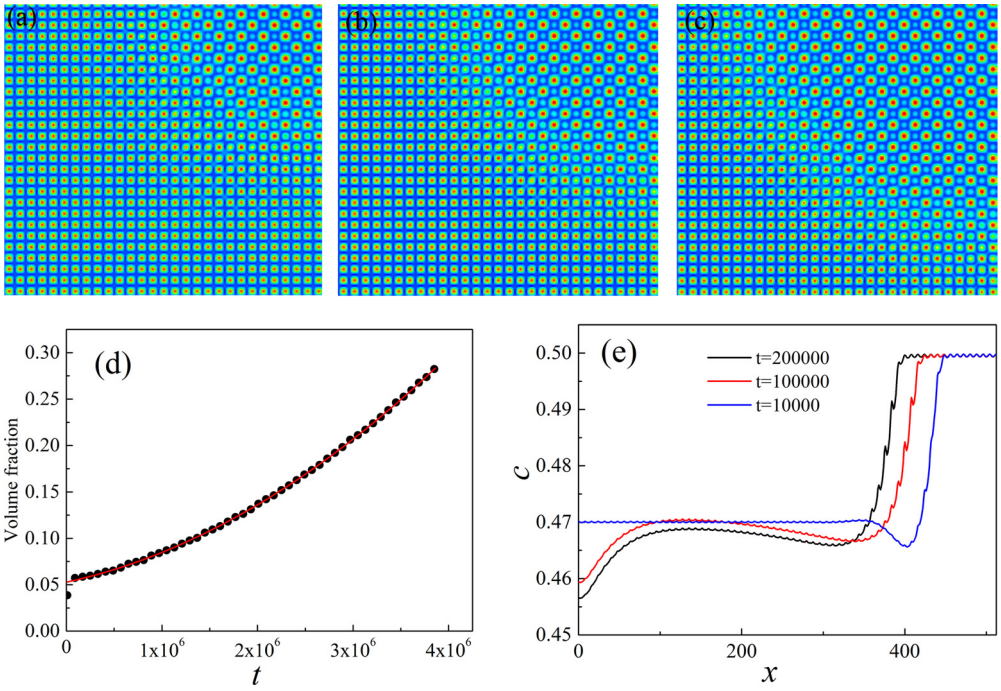


FIG. 5. Simulated results of the ordered precipitate growth process at $c_0 = 0.47$, $\sigma = 0.05$. (a)–(c) show the evolution of the $\eta$ field at $t = 10\,000$, 100 000, and 200 000, respectively; (d) shows the variation of precipitate volume fraction with time; (e) shows the concentration profiles across the interface.

precipitation is controlled by diffusion. Figure 5(e) shows the concentration profiles across the interface. Because the matrix is supersaturated, the chemical potential of the matrix is higher than that for the ordered domain, resulting in the flux of $B$ atoms toward the growing particle, as shown in Fig. 5(e). The change of composition makes $C_2^{\text{order}}$ in $C_{\text{eff}}^n(|r-r'|)$ gradually work and then drives the evolution of $\eta$, leading to the occurrence of an order-disorder transition.

### B. Evolution of antiphase domain and antiphase domain boundary

Another important feature for order-disorder transitions is the evolution of antiphase domains (APDs) [10] which determine the strengthening mechanisms and deformation behaviors of ordered phases. As we know, if two APDs impinge with each other during the growth or coarsening process, they will not merge directly but a structural defect called antiphase domain boundary (APB) will be generated. To examine the capability of our approach in describing order-disorder phase transitions, the evolution of APDs and the energy of APBs are checked. The width of APBs can be changed by varying the width of Gaussian peak $\alpha$ in Eq. (12) and thus the free energy of APBs. The relationship between the width $W$ of APB and the peak width $\alpha$ is shown in Fig. 6(a). It shows that $W$ decreases almost linearly with the increase of $\alpha$. Figure 6(b) shows the interface energy of APB $\gamma_{\text{APB}}$ and that for the order-disorder interfacial boundaries $\gamma_{\text{order-disorder}}$ vs the peak width $\alpha$. It shows that, when $\alpha \leqslant 0.7$, $\gamma_{\text{APB}}$ is higher than twice of $\gamma_{\text{order-disorder}}$, so in this case APBs will decompose into two single-domain particles separated by a thin layer of the disordered phase. When $\alpha \geqslant 0.8$, APBs can be stable.

Figure 7 shows the growth and coarsening process of APDs when $\alpha = 0.4$. The initial condition consists of two small spherical particles of the ordered structure with a radius of $8a_{\text{sq}}$. The two ordered domains are next to each other but separated by an APB. Such an initial configuration turns out to be unstable because APB is unstable in this case, as shown in Figs. 7(a)–7(c). The APDs transformed into two single-domain particles separated by a thin layer of disordered phase, and the APB is replaced by two order-disorder interfacial boundaries and a layer of the disordered phase eventually. Figure 7(d) shows the concentration change across the interface. The concentration of the disordered phase between the two APDs is a bit lower than that of APDs.

Figure 8 shows the variation of $\gamma_{\text{APB}}$ with the temperature parameter $\sigma$ when the width of the correlation function $\alpha = 0.8$ (the black line). For comparison, the variation of $\gamma_{\text{APB}}$ in the Ni-Al system with temperature calculated by the cluster variation method (CVM) [34] (the red line) is also shown in Fig. 8. It shows that the $\gamma_{\text{APB}}$ first increases with $\sigma$ and then decreases a little bit, which has a similar tendency with the calculated results by CVM. This nonmonotonic temperature dependence of the interface energy has also been confirmed by M. Asta *et al.* in their study of fcc substitutional alloys [35]. The similar tendency of APB energy also shows the capability of our approach.

With the two case studies, we have demonstrated the capabilities of our approach in describing the order-disorder transition. With the approach, the PFC model can describe the properties of ordered and disordered structures and APB very well. With the improved model, we can deal with the problems on atomic length scales and diffusional time scales.

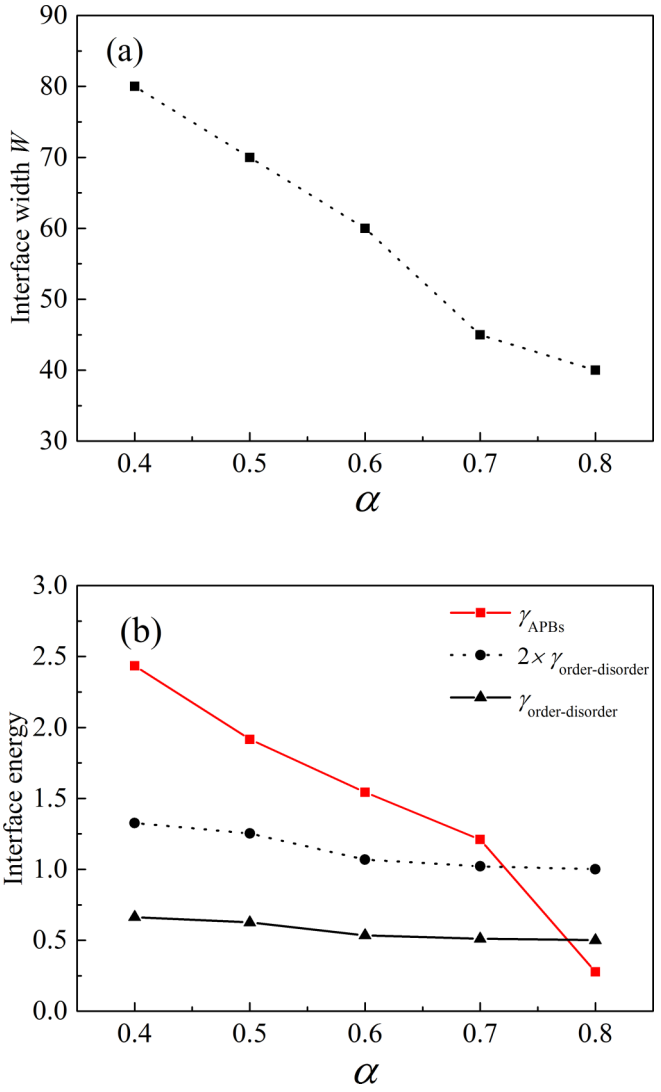


FIG. 6. (a) The interface width $W$ as a function of the peak width $\alpha$; (b) the variation of APB energy (a) and order-disorder interface energy (b) with the peak width $\alpha$.

## IV. DISCUSSION AND CONCLUSION

We have introduced an approach to describe order-disorder transitions based on the PFC model. This approach is very similar to the model introduced by Alster *et al.* [27]. Both works add the long-range information into the original PFC model. But the origins of the two approaches are different. Our approach is inspired from the different image intensities between superlattices of ordered structures in HRTEM images. So we add a new periodic order parameter into the PFC model. This periodic order parameter in our model can reflect the fundamental lattices and the difference between superlattices of ordered structures. However, Alster *et al.* used the concentration wave as the order parameter to represent ordered structures. In the model by Alster *et al.*,

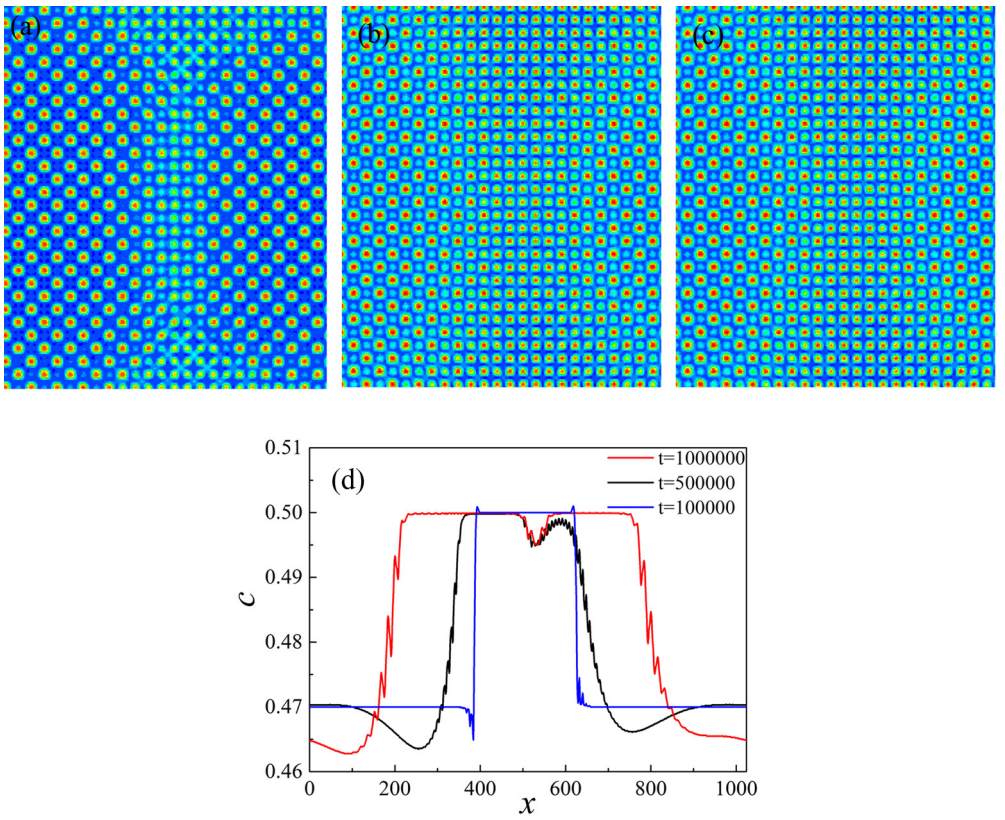


FIG. 7. Evolution of APD when $c_0 = 0.47$, $\sigma = 0.05$. (a)–(c) show the atomic image at $t = 10\,000$, 1 000 000, and 2 000 000, respectively; (d) shows the concentration profiles at different times.

the periodic concentration field reflects the difference between superlattices, while the periodic atomic density field reflects the fundamental lattices of ordered structures. These two approaches would bring several differences in use. Probably the most outstanding example is in studying the problems of the elastic-plastic deformations of ordered structures for the two models. In our model, because the concentration field is uniform, the elastic-plastic behaviors are mainly described through the changes of the single periodic field. But in the model by Alster *et al.*, the elastic-plastic behaviors are described through the changes of the two periodic fields: the atomic density field and the concentration field. So if someone uses the model by Alster *et al.* to study the problems of the elastic-plastic deformations of ordered structures, he needs to take into account the coupling of the two periodic fields.

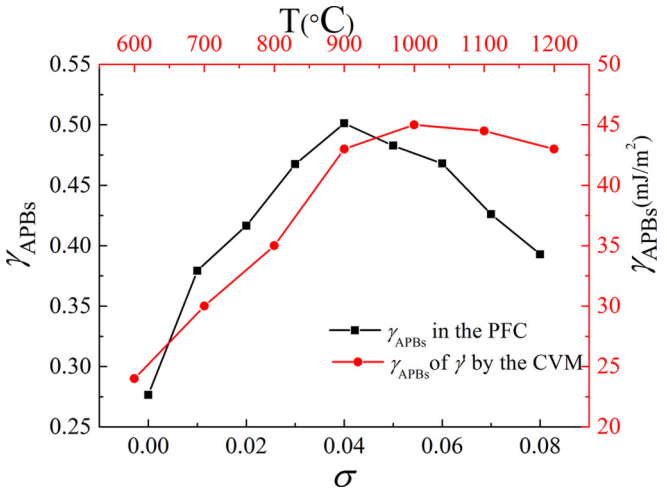


FIG. 8. Effect of temperature $\sigma$ on the interface energy of APBs at $\alpha = 0.8$ (the black line); the red line shows the $\gamma_{APB}$ of $\gamma'$ vs temperature in the Ni-Al system by using the CVM [34].

In summary, we have developed an approach to describe order-disorder phase transitions on atomic length scales and diffusional time scales. Based on the original PFC model, we added an order parameter $\eta$ to reflect the atomic potential distribution inspired from HRTEM. This new order parameter $\eta$ includes the information about the regular arrangements of atoms in ordered structures, and thus can be used to describe order-disorder systems. Considering the physical fact that long-range interactions of atoms exist in ordered structures but disappear in disordered structures, we constructed the correlation function with two parts: one works on the fundamental lattice and one works on the superlattice. From presenting 2D and 3D ordered structures, and two case studies including the growth of ordered precipitations and evolution of antiphase domains, we demonstrated the capabilities and potential applications of our approach. The improved model can be used to deal with the issues in order-disorder systems on atomic length scales and diffusional time scales, such as microstructure evolution, strengthening mechanisms, and deformation behaviors of ordered phases.

**ACKNOWLEDGMENTS**

The work was supported by National Natural Science Foundation of China (Grants No. 51571165 and No. 51371151), Special Pprogram for Applied Research on Super Computation of the NSFC-Guangdong Joint Fund (the second phase). We also thank the Center for High Performance Computing of Northwestern Polytechnical University, China for computer time and facilities.

[1] A. G. Khachaturyan, Ordering in substitutional and interstitial solid solutions, Prog. Mater. Sci. **22**, 1 (1978).

[2] M. Phani, J. L. Lebowitz, M. Kalos, and O. Penrose, Kinetics of an Order-Disorder Transition, Phys. Rev. Lett. **45**, 366 (1980).

[3] G. F. Mazenko, O. T. Valls, and F. Zhang, Kinetics of first-order phase transitions: Monte Carlo simulations, renormalization-group methods, and scaling for critical quenches, Phys. Rev. B **31**, 4453 (1985).

[4] X. Shao, Z. Yang, and X. Ma, Strengthening and toughening mechanisms in Mg–Zn–Y alloy with a long period stacking ordered structure, Acta Mater. **58**, 4760 (2010).

[5] M. Kerr and N. Chawla, Creep deformation behavior of Sn–3.5 Ag solder/Cu couple at small length scales, Acta Mater. **52**, 4527 (2004).

[6] W. L. Bragg and E. Williams, The effect of thermal agitation on atomic arrangement in alloys, Proc. R. Soc. London, Ser. A **145**, 699 (1934).

[7] W. L. Bragg and E. J. Williams, The effect of thermal agitation on atomic arrangement in alloys. II, Proc. R. Soc. London, Ser. A **151**, 540 (1935).

[8] F. Cleri, G. Mazzone, and V. Rosato, Order-disorder transition in Cu 3 Au: A combined molecular-dynamics and cluster-variation-method approach, Phys. Rev. B **47**, 14541 (1993).

[9] A. G. Khachaturyan, *Theory of Structural Transformations in Solids* (Courier Corporation, North Chelmsford, MA, 2013).

[10] Y. Wang, D. Banerjee, C. Su, and A. Khachaturyan, Field kinetic model and computer simulation of precipitation of $L1_2$ ordered intermetallics from f.c.c. solid solution, Acta Mater. **46**, 2983 (1998).

[11] L.-Q. Chen, Phase-field models for microstructure evolution, Ann. Rev. Mater. Res. **32**, 113 (2002).

[12] K. R. Elder and M. Grant, Modeling elastic and plastic deformations in nonequilibrium processing using phase field crystals, Phys. Rev. E **70**, 051605 (2004).

[13] K. Elder, N. Provatas, J. Berry, P. Stefanovic, and M. Grant, Phase-field crystal modeling and classical density functional theory of freezing, Phys. Rev. B **75**, 064107 (2007).

[14] M. Greenwood, N. Provatas, and J. Rottler, Free Energy Functionals for Efficient Phase Field Crystal Modeling of Structural Phase Transformations, Phys. Rev. Lett. **105**, 045702 (2010).

[15] A. Jaatinen and T. Ala-Nissila, Eighth-order phase-field-crystal model for two-dimensional crystallization, Phys. Rev. E **82**, 061602 (2010).

[16] P. Y. Chan, N. Goldenfeld, and J. Dantzig, Molecular dynamics on diffusive time scales from the phase-field-crystal equation, Phys. Rev. E **79**, 035701 (2009).

[17] G. Kocher and N. Provatas, New Density Functional Approach for Solid-Liquid-Vapor Transitions in Pure Materials, Phys. Rev. Lett. **114**, 155501 (2015).

[18] E. J. Schwalbach, J. A. Warren, K.-A. Wu, and P. W. Voorhees, Phase-field crystal model with a vapor phase, Phys. Rev. E **88**, 023306 (2013).

[19] G. I. Tóth, G. Tegze, T. Pusztai, and L. Gránásy, Heterogeneous Crystal Nucleation: The Effect of Lattice Mismatch, Phys. Rev. Lett. **108**, 025502 (2012).

[20] B. P. Athreya, N. Goldenfeld, J. A. Dantzig, M. Greenwood, and N. Provatas, Adaptive mesh computation of polycrystalline pattern formation using a renormalization-group reduction of the phase-field crystal model, Phys. Rev. E **76**, 056706 (2007).

[21] V. Fallah, A. Korinek, N. Ofori-Opoku, B. Raeisinia, M. Gallerneault, N. Provatas, and S. Esmaeili, Atomic-scale pathway of early-stage precipitation in Al–Mg–Si alloys, Acta Mater. **82**, 457 (2015).

[22] M. Seymour and N. Provatas, Structural phase field crystal approach for modeling graphene and other two-dimensional structures, Phys. Rev. B **93**, 035447 (2016).

[23] M. Greenwood, N. Ofori-Opoku, J. Rottler, and N. Provatas, Modeling structural transformations in binary alloys with phase field crystals, Phys. Rev. B **84**, 064104 (2011).

[24] J. Berry and M. Grant, Modeling Multiple Time Scales During Glass Formation with Phase-Field Crystals, Phys. Rev. Lett. **106**, 175702 (2011).

[25] J. Berry and M. Grant, Phase-field-crystal modeling of glass-forming liquids: Spanning time scales during vitrification, aging, and deformation, Phys. Rev. E **89**, 062303 (2014).

[26] P. Y. Chan, Scaling and pattern formation in condensed matter systems, Ph.D. thesis, University of Illinois at Urbana-Champaign, 2007.

[27] E. Alster, K. Elder, J. J. Hoyt, and P. W. Voorhees, Phase-field-crystal model for ordered crystals, Phys. Rev. E **95**, 022105 (2017).

[28] J. Chen, E. Costan, M. Van Huis, Q. Xu, and H. Zandbergen, Atomic pillar-based nanoprecipitates strengthen AlMgSi alloys, Science **312**, 416 (2006).

[29] L. Kovarik, P. Gouma, C. Kisielowski, S. Court, and M. Mills, A HRTEM study of metastable phase formation in Al–Mg–Cu alloys during artificial aging, Acta Mater. **52**, 2509 (2004).

[30] Z.-A. Li, M. Spasova, Q. Ramasse, M. Gruner, C. Kisielowski, and M. Farle, Chemically ordered decahedral FePt nanocrystals observed by electron microscopy, Phys. Rev. B **89**, 161406 (2014).

[31] V. Fallah, A. Korinek, N. Ofori-Opoku, N. Provatas, and S. Esmaeili, Atomistic investigation of clustering phenomenon in the Al–Cu system: Three-dimensional phase-field crystal simulation and HRTEM/HRSTEM characterization, Acta Mater. **61**, 6372 (2013).

[32] D. B. Williams and C. B. Carter, *Transmission Electron Microscopy* (Springer, New York, 1996), Chap. 1, pp. 3–17.

[33] M. Greenwood, J. Rottler, and N. Provatas, Phase-field-crystal methodology for modeling of structural transformations, Phys. Rev. E **83**, 031601 (2011).

[34] J. C. Wang, M. Osawa, T. Yokokawa, H. Harada, and M. Enomoto, Interface energy calculation of $\gamma$-$\gamma'$ in Ni-Al system using the cluster variation method, *Materials Science Forum* (Trans. Tech. Publ., Zurich, 2007), Vol. 546, pp. 1333–1338.

[35] M. Asta, Thermodynamic properties of coherent interphase boundaries in fcc substitutional alloys, *Theory and Applications of the Cluster Variation and Path Probability Methods* (Springer, New York, 1996), pp. 237–254.